V European Conference on Computational Fluid Dynamics
ECCOMAS CFD 2010
J. C. F. Pereira and A. Sequeira (Eds)
Lisbon, Portugal, 14–17 June 2010

STREAMLINES OF VORTICAL FLOWS IN 3D LID-DRIVEN CAVITIES

Katsuya Ishii[*] and Shizuko Adachi[†]

[*] Information Technology Center, Nagoya University
Furo-cho, Chikusa-ku, Nagoya 464-8601, Japan
e-mail: ishii@itc.nagoya-u.ac.jp

[†]School of Business and Commerce, Tokyo International University
1-13-1 Matoba-kita, Kawagoe, Saitama 350-1197, Japan
e-mail: sadachi@tiu.ac.jp

Key words: Cavity flow, Three-dimensional Steady flow, Streamline, Poincaré section

Abstract. *Streamlines of the incompressible vortical flows in three-dimensional rectangular cavities are numerically studied for several Reynolds numbers by using a combined compact finite difference(CCD) scheme with high accuracy and high resolution. The flow is driven by a lid moving tangentially with constant speed. Non-dimensional geometrical parameters of the cavity are the depth-to-width aspect ratio Γ and the span-to-width aspect ratio Λ. The flow parameter is the Reynolds number Re. We study the flow structure in the square cavity(Γ=1) with the spanwise aspect ratio Λ=6.55 for Re from 100 to 400. Streamlines are obtained from the velocity field of the steady incompressible flow. Several streamlines show chaotic behaviour, and in certain cases there is a closed streamline on a torus. In order to examine the features of particle paths we plot the Poincaré sections.*

1 INTRODUCTION

Flows in a lid-driven cavity display a lot of interesting physical phenomena in fluid mechanics. There have been many studies[1] of the internal flows in the closed system with the simplest geometry because they are of fundamental importance as well as of practical importance.

The sketch of the coordinate system of a three-dimensional lid-driven cavity, which has width H, depth D and span L, is presented in Fig.1. The upper wall(y=1) moves in x-direction with constant speed U. Non-dimensional geometrical parameters of the cavity are the aspect ratio $\Gamma=D/H$ and the spanwise aspect ratio $\Lambda=L/H$. The flow parameter is the Reynolds number $Re=U/Hv$ where v is the kinematic viscosity.

A lot of papers have been published on three-dimensional cavity flows. Almost all the work are for a square cavity(Γ=1), and among them papers for long-span cavities are not many. Albensoeder *et al*. studied the flow in a cavity with Γ=1 and Λ=6.55 both experimentally and computationaly. For Re=850 Albensoeder *et al*.[2] found that Taylor-Görtler vortices can exist in the middle of the cavity around the center plane and that the Taylor-Görtler vortices are suppressed in the near-wall regions. Albensoeder and Kuhlmann[3] later presented the numerical results which agree qualitatively with the experimental ones. The Taylor-Görtler vortices breaks down at Re=835±5 when the Reynolds number is reduced quasi-statically. This Reynolds number is about 6% larger than the critical Reynolds number obtained by a linear stability analysis for an infinitely long-span system with periodic boundary conditions.

Streamlines and Poincaré sections help us to examine characteristic features of three-dimensional cavity flows. Ishii *et al.*[4] studied the streameline structure in the steady flow fields in a cubic cavity($\Gamma=\Lambda$=1) for Re from 100 to 400. They showed that Poincaré sections of the streamlines present various structures of invariant curves, resonant islands and chaotic distribution. In the previous numerical study[5] of the steady flows in a square cavity with Λ=6.55 at Re=850, we also found a cell structure in the center region. The present work is intended to study the three-dimensional features in the center region and in the near-wall regions of cavities with a long span for Re from 100 to 850, and to investigate the difference between the regions with the cell structure and other regions. In the present paper we report the results of numerical simulations for the incompressible steady flows in a square cavity with Λ=6.55 for Re from 100 to 400. Streamlines and Poincaré sections are presented and they are compared with those obtained from the previous study of the flow in a cubic cavity by Ishii *et al.*

The problem is formulated in Sect.2, and numerical methods are described in Sect.3. After the results are presented in Sect.4, conclusions are given in the last section.

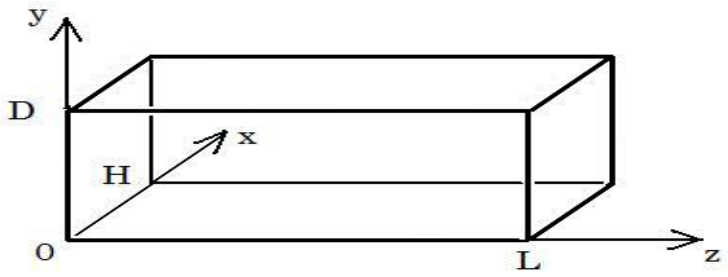

Figure 1: Coordinate system.

2 FORMULATION

We consider the flow of an incompressible fluid with constant density ρ in a three-dimensional lid-driven cavity. We study the flow structure in a square cavity(Γ=1) with a spanwise aspect ratio Λ=6.55 at *Re* = 100 and 300.

The governing equations are the three-dimensional incompressible Navier-Stokes equations

$$\frac{\partial \mathbf{u}}{\partial t} + \mathbf{u} \cdot \nabla \mathbf{u} = -\nabla p + \frac{1}{Re} \nabla^2 \mathbf{u}, \tag{1}$$

$$\nabla \cdot \mathbf{u} = 0, \tag{2}$$

where lengths, time, velocities and pressure are made dimensionless using H,U and ρ. The boundary conditions are

$$\mathbf{u} = (1,0,0) \text{ at } y = 1,$$
$$\mathbf{u} = \mathbf{0} \text{ at } y = 0,$$
$$\mathbf{u} = \mathbf{0} \text{ at } x = 0 \text{ and } 1,$$
$$\mathbf{u} = \mathbf{0} \text{ at } z = 0 \text{ and } \Lambda.$$

The boundary condition for the derivative is obtained from the above boundary conditions for **u** and the continuity equation

$$\left.\frac{\partial u_n}{\partial n}\right|_{wall} = 0,$$

where n denotes the normal direction to the wall.

3 NUMERICAL METHODS

Since the flows in lid-driven cavities have different spatial scales, it is essential to use schemes with high accuracy and high resolution in the numerical simulations[6]. We therefore adopt the the Combined Compact Difference (CCD) method with spectral-like resolution which was developed by Nihei and Ishii[7,8].

3.1 A CCD scheme

Consider a function $f(x)$ defined on the interval where N grid points are located with a uniform spacing h. Let f_i, f_i', f_i'' and f_i''' be the values of the function and its first, second and third derivatives at i-th grid point respectively. The CCD scheme gives a linear algebraic system of equations for the function and its first, second and third derivatives at three neighboring points

$$f_i' + a_1(f_{i+1}' + f_{i-1}') + b_1 h(f_{i+1}'' - f_{i-1}'') + c_1 h^2(f_{i+1}''' + f_{i-1}''') = \frac{d_1}{h}(f_{i+1} - f_{i-1}),$$

$$f_i'' + \frac{a_2}{h}(f_{i+1}' - f_{i-1}') + b_2(f_{i+1}'' + f_{i-1}'') + c_2 h(f_{i+1}''' - f_{i-1}''') = \frac{d_2}{h^2}(f_{i+1} - 2f_i + f_{i-1}),$$

$$f_i''' + \frac{a_3}{h^2}(f_{i+1}' + f_{i-1}') + \frac{b_3}{h}(f_{i+1}'' - f_{i-1}'') + c_3(f_{i+1}''' + f_{i-1}''') = \frac{d_3}{h^3}(f_{i+1} - f_{i-1}).$$

The coefficients of the linear system of equations are determined so that the CCD scheme has high accuracy and high resolution at the same time.

The present CCD scheme has 8-th order accuracy for the first derivative at inner points and 5-th order accuracy for the first derivative at the boundary. When the first derivative is given at the boundary, the scheme has 5-th accuracy for the second derivative.

The linear system of equations is written in matrix form

$$\begin{pmatrix} \mathbf{B}_1 & \mathbf{C}_1 & \mathbf{0} & \mathbf{0} & \cdots & \mathbf{0} & 0 \\ \mathbf{A} & \mathbf{B} & \mathbf{C} & \mathbf{0} & \cdots & \mathbf{0} & \mathbf{0} \\ \mathbf{0} & \mathbf{A} & \mathbf{B} & \mathbf{C} & & \mathbf{0} & \mathbf{0} \\ \vdots & & \ddots & \ddots & \ddots & & \vdots \\ \mathbf{0} & \mathbf{0} & & \mathbf{A} & \mathbf{B} & \mathbf{C} & \mathbf{0} \\ \mathbf{0} & \mathbf{0} & \cdots & \mathbf{0} & \mathbf{A} & \mathbf{B} & \mathbf{C} \\ 0 & \mathbf{0} & \cdots & \mathbf{0} & \mathbf{0} & \mathbf{A}_N & \mathbf{B}_N \end{pmatrix} \begin{pmatrix} \mathbf{x}_1 \\ \mathbf{x}_2 \\ \mathbf{x}_3 \\ \vdots \\ \mathbf{x}_i \\ \vdots \\ \mathbf{x}_N \end{pmatrix} = \begin{pmatrix} \mathbf{d}_1 \\ \mathbf{d}_2 \\ \mathbf{d}_3 \\ \vdots \\ \mathbf{d}_i \\ \vdots \\ \mathbf{d}_N \end{pmatrix}.$$

We solve this block tridiagonal system of equations to obtain the derivatives.

Matrices and vectors in the equation are

$$\mathbf{A} = \begin{pmatrix} a_1 & -b_1 & c_1 \\ -a_2 & b_2 & -c_2 \\ a_3 & -b_3 & c_3 \end{pmatrix}, \ \mathbf{B} = \begin{pmatrix} 1 & 0 & 0 \\ 0 & 1 & 0 \\ 0 & 0 & 1 \end{pmatrix}, \ \mathbf{C} = \begin{pmatrix} a_1 & b_1 & c_1 \\ a_2 & b_2 & c_2 \\ a_3 & b_3 & c_3 \end{pmatrix},$$

$$\mathbf{x}_i = \begin{pmatrix} hf_i' \\ h^2 f_i'' \\ h^3 f_i''' \end{pmatrix}, \ \mathbf{d}_i = \begin{pmatrix} d_1(f_{i+1} - f_{i-1}) \\ d_2(f_{i+1} - 2f_i + f_{i-1}) \\ d_3(f_{i+1} - f_{i-1}) \end{pmatrix},$$

for inner points, and we use the following parameters

$$a_1 = \frac{8d_3 + 195}{240}, b_1 = -\frac{16d_3 + 255}{1200}, c_1 = \frac{4d_3 + 45}{96}, d_1 = \frac{8d_3 + 315}{240},$$

$$a_2 = \frac{11d_2 - 15}{16}, b_2 = -\frac{3d_2 - 7}{16}, c_2 = \frac{d_2 - 3}{48},$$

$$a_3 = d_3, b_3 = -\frac{8d_3 + 15}{20}, c_3 = \frac{4d_3 + 15}{60},$$

$$d_2 = 9.12992, \ d_3 = -6.01486.$$

3.2 A Poisson solver

The Marker-and-Cell(MAC) method is used in solving the governing equations. In the MAC method, the Poisson equation for pressure needs to be solved in place of the continuity equation,

$$\nabla^2 p = q, \tag{3}$$

where

$$q = -\frac{\mathrm{div}\mathbf{u}^n}{\Delta t} + \nabla\nabla : \mathbf{u}^n\mathbf{u}^n + \frac{1}{Re}\nabla^2 \mathrm{div}\mathbf{u}^n$$

at the *n*-th time step for the momentum equation, and the boundary condition on the wall is

$$\nabla p\big|_{wall} = \frac{1}{Re}\nabla^2 \mathbf{u}^n.$$

In order to solve the Poisson equation, we include an artificial term which vanishes when the steady-state solution is reached

$$\frac{\partial p}{\partial \tau} = \nabla^2 p - q, \tag{4}$$

where τ is a fictitious time. The Crank-Nicolson form of this equation is

$$p^{m+1} - p^m = \Delta\tau\left\{\frac{\left(\nabla^2 p\right)^{m+1} + \left(\nabla^2 p\right)^m}{2} - q\right\}, \tag{5}$$

and this is transformed into

$$\left(1 - \frac{\Delta\tau}{2}\left(\partial_x^2 + \partial_y^2 + \partial_z^2\right)\right)\left(p^{m+1} - p^m\right) = \Delta\tau\left\{\left(\partial_x^2 + \partial_y^2 + \partial_z^2\right)p^m - q\right\}, \tag{6}$$

where p^{m+1} is the value of p at the (m+1)-th step in solving eq.(5). When we apply an approximate factorization scheme to eq.(6), we obtain

$$\left(1 - \frac{\Delta\tau}{2}\partial_x^2\right)\left(1 - \frac{\Delta\tau}{2}\partial_y^2\right)\left(1 - \frac{\Delta\tau}{2}\partial_z^2\right)\left(p^{m+1} - p^m\right) = \Delta\tau\left\{\left(\partial_x^2 + \partial_y^2 + \partial_z^2\right)p^m - q\right\}.$$

We solve this equation using a three-step scheme given by

Step1: $P^* - \frac{\Delta\tau}{2}\partial_x^2 P^* = \Delta\tau\left\{\left(\partial_x^2 + \partial_y^2 + \partial_z^2\right)p^m - q\right\}$ and CCD equations in x-direction,

Step 2: $P^{**} - \frac{\Delta\tau}{2}\partial_y^2 P^{**} = P^*$ and CCD equations in y-direction,

Step 3: $P^{***} - \frac{\Delta\tau}{2}\partial_z^2 P^{***} = P^{**}$ and CCD equations in z-direction,

where P^* and P^{**} are intermediate values

$$P^* = \left(1 - \frac{\Delta\tau}{2}\partial_y^2\right)\left(1 - \frac{\Delta\tau}{2}\partial_z^2\right)\left(p^{m+1} - p^m\right), P^{**} = \left(1 - \frac{\Delta\tau}{2}\partial_z^2\right)\left(p^{m+1} - p^m\right),$$

and

$$P^{***} = p^{m+1} - p^m.$$

The equations for P^* and its first, second and third derivatives are solved at Step 1. With the intermediate value of P^* the equations for P^{**} and its first, second and third derivatives are solved at Step 2. Then using the intermediate value of P^{**} the equations for P^{***} and its first, second and third derivatives are solved at Step 3. The final value p^{m+1} of the (m+1)-th step is given by

$$p^{m+1} = p^m + P^{***}.$$

We stop the iteration for eq. (5) when

$$\left\|\left(\nabla^2 p - q\right)/\, q\right\| < \varepsilon_p,$$

where $\varepsilon_p = 1\times10^{-6}$.

After the Poisson equation for pressure is solved, we evaluate the value of the right hand side of the momentum equation (1) for the next step. We use a criterion

$$\left\|\Delta u / \Delta t\right\| < \varepsilon$$

for the convergence to the steady state, where $\varepsilon = 5\times10^{-5}$.

4 RESULTS

In the present numerical simulation the 101×101×656 uniform grid system is used and the time step for the momentum equation is $\Delta t = 1\times10^{-3}$.

4.1 Poincaré section

Streamlines are obtained from the velocity field of the steady incompressible flow. We present Poincaré sections of twenty streamlines at *Re* = 100, 300 and 400 in Figs. 2, 3 and 4 respectively. Dots in the map indicate positions where a certain streamline

intersects the plane of x=0.5 in the direction of negative x. The left half of the cavity is presented in the figures. The left side is the end wall and the right side is the center plane z=3.275.

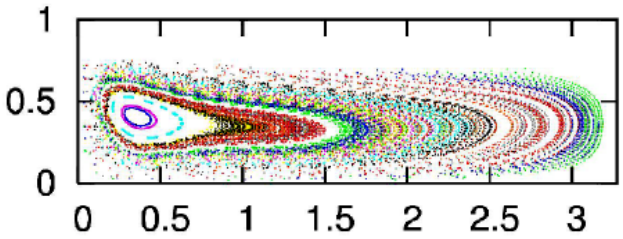

Figure 2: Poincaré section on x = 0.5 for Re = 100.

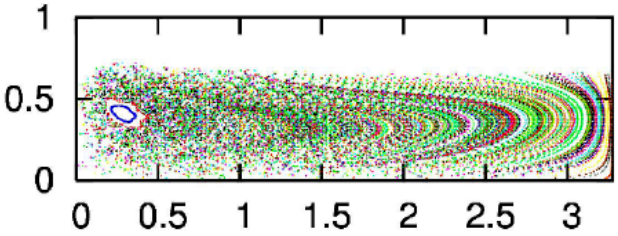

Figure 3: Poincaré section on x = 0.5 for Re = 300.

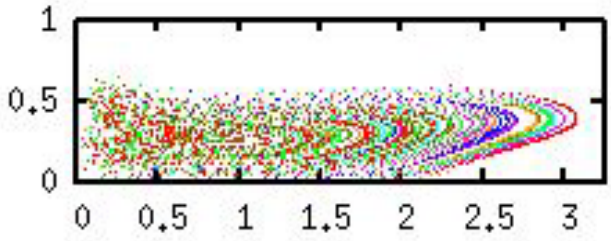

Figure 4: Poincaré section on x = 0.5 for Re = 400.

In the Poincaré section for Re=100 in Fig. 2, we find many points which form three ovals surrounding a fixed point at around z = 0.4. The points on each oval are intersections by one closed streamline. This structure of streamlines in the steady flow is similar to that at Re=100 of the flow in the cubic cavity. In the Poincaré section for Re=300 in Fig. 3, only one closed dotted curve by a streamline can be found at around z = 0.3. Other points in the Poincaré sections in Figs. 2 and 3 correspond to chaotic motion. In the case of the cubic cavity, any well-defined closed curve cannot be found in the Poincaré section at Re > 335. In the Poincaré section for Re=400 in Fig. 4, we cannot find any oval near the end wall also in the long-span cavity, and there is an area in the lower central region (z=2.5-3.275) where streamlines of chaotic motion do not enter. The spanwise velocity component is small in this region.

4.2 Streamlines

Typical streamlines for Re=100 are presented in Figs. 5 and 6. The streamline in Fig.5 corresponds to one oval surrounding a point at around z = 0.4 in Fig. 2.

Figure 5: A localized streamline for *Re* = 100.

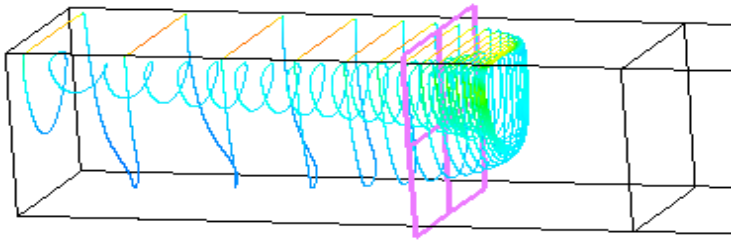

Figure 6: An extending streamline for *Re* = 100.

The streamline in Fig. 6 corresponds to points of chaotic motion in the Poincaré section in Fig. 2. The streamline starts from the plane presented in the figure, and it moves towards the left end wall in a large spiral, then it moves towards the center plane along the axis of the primary vortex in a small spiral. Near the center plane it spirals outwards. The streamlines of chaotic motion do not enter the torus presented in Fig. 5.

Figure 7: A localized streamline for *Re* = 300.

The streamline in Fig. 7 corresponds to a closed dotted curve at around z = 0.3 in Fig.3 for *Re*=300. Figures are not presented for *Re*=300 but there are streamlines corresponding to chaotic motion which are similar to the streamline in Fig. 6.

5 CONCLUSIONS

We studied the global flow structure in a square cavity with a spanwise aspect ratio Λ=6.55 at *Re* from 100 to 400. In order to simulate numerically the flows with different spatial scales we used a spectral-like combined compact finite difference (CCD) scheme with high accuracy and high resolution. A closed streamline on a torus is found at *Re* = 100 and 300, and it is not found at *Re*=400. Several streamlines show chaotic behaviour. Those streamlines extend from the center to the end wall of the cavity, which shows that the flow is not two-dimesional in the center region of a long cavity with Λ=6.55. Even in the relatively low Reynolds number range *Re* from 100 to 400, the nature of the cavity flow is three-dimensional.

ACKNOWLEDGEMENT

This work was supported by a Grant-in-Aid for Scientific Research from Japan Society for the Promotion of Science. Computer resources were provided by the Information Technology Center of Nagoya University.

REFERENCES

[1] P.N. Shankar and M.D. Deshpande, Fluid mechanics in the Driven Cavity, *Annu. Rev. Fluid Mech.*, **32**, 93-136 (2000).

[2] S. Albensoeder, H.C. Kuhlmann and H.J. Rath, Three-dimensional centrifugal-flow instabilities in the lid-driven cavity problem, *Phys. Fluids.***13**, 121-135 (2001).

[3] S. Albensoeder and H.C. Kuhlmann, Nonlinear three-dimensional flow in the lid-driven square cavity, *J. Fluid Mech*. **569**, 465-480 (2006).

[4] K. Ishii and R. Iwatsu, Numerical simulation of the Lagrangian flow structure in a driven-cavity, Topological Fluid Mechanics, H.K.Moffatt and A. Tsinobar Eds., *Cambridge Univ. Press*, 54-63 (1990).

[5] K. Ishii and S. Adachi, Numerical analysis of 3D vortical cavity flow. *PAMM* **Vol. 6**, 871-874 (2007)

[6] K. Ishii, T. Nihei and S. Adachi, Accurate Numerical Simulation of Three-dimensional Lid-driven Cavity Flows with Different Span Length, Vortex Dominated Flows, D.Blackmore, E.Krause and C.Tung Eds., *World Scientific Publishing*, 87-96 (2005).

[7] Tomonori Nihei and Katsuya Ishii, A fast solver of the shallow water equations on a sphere using a combined compact difference scheme, *J. Comput. Phys.* **187**, 639-659 (2003)

[8] Tomonori Nihei and Katsuya Ishii, Parallelization of a Highly Accurate Finite Difference Scheme for Fluid Flow Calculations, *Theoretical and Applied Mechanics Japan* **52**, 71-81 (2003)